Cryogenic 3D Printing of Porous Scaffolds for *in situ* Delivery of 2D Black Phosphorus Nanosheets, Doxorubicin Hydrochloride and Osteogenic Peptide for Treating Tumor Resection-Induced Bone Defects

Chong Wang[1,†,*], Xinyu Ye[2,†], Yitao Zhao[3,†], Lu Bai[4], Zhi He[1], Qing Tong[1], Xiaoqiong Xie[1], Huangrong Zhu[3], Daozhang Cai[3], Yun Zhou[5], Bingheng Lu[1],Yen Wei[6], Lin Mei[5,*], Denghui Xie[3,*], Min Wang[7]

[1]College of Mechanical Engineering, Dongguan University of Technology, Dongguan, Guangdong, P.R. China

[2]School of Medicine, Southern University of Science and Technology, Shenzhen, Guangdong, P.R. China

[3]Department of Orthopedic Surgery, The Third Affiliated Hospital of Southern Medical University, Academy of Orthopedics, Guangzhou, Guangdong, P.R. China

[4]Department of Sports Medicine Shenzhen Hospital of Peking University, Shenzhen, Guangdong, P.R. China

[5]School of Pharmaceutical Sciences (Shenzhen), Sun Yat-sen University, Guangzhou, Guangdong, P.R. China

[6]Department of Chemistry, Tsinghua University, Beijing, P.R. China

[7]Department of Mechanical Engineering, The University of Hong Kong, Pokfulam Road, Hong Kong, P.R. China

Keywords: *cryogenic 3D printing; osteogenic peptide; black phosphorus nanosheets; doxorubicin hydrochloride; cancer recurrence; bone regeneration*

---

*Correspondences: Dr. Chong Wang, wangchong@dgut.edu.cn; Prof. Lin Mei, meilin7@mail.sysu.edu.cn; Dr. Denghui Xie, smuspine@163.com; C. W.[†], X. Y.[†] and Y. Z.[†] contributed equally.

ABSTRACT

Tumor resection is widely used to prevent tumor growth. However, the defected tissue at the original tumor site also causes tissue or organ dysfunction which lowers the patient's life quality. Therefore, regenerating the tissue and prevent tumor recurrence are highly important. Herein, according to the concept of "first kill and then regenerate", a versatile scaffold-based tissue engineering strategy based on cryogenic 3D printing of water-in-oil polyester emulsion inks containing multiple functional agents was developed,in order to realize the elimination of tumor cells with recurrence suppression and improved tissue regeneration sequentially. To illustrate our strategy, water/poly(lactic-co-glycolic acid)/dichloromethane emulsions containing β-tricalcium phosphate (β-TCP), 2D black phosphorus (BP) nanosheets, low-dose doxorubicin hydrochloride (DOX) and high-dose osteogenic peptide were cryogenically 3D printed into hierarchically porous and mechanically strong nanocomposite scaffolds,with multiple functions to treat bone tumor resection-induced tissue defects. Prompt tumor ablation and long-term suppression of tumor recurrence could be achieved due to the synergistic effects of photothermotherapy and chemotherapy, and improved bone regeneration was obtained eventually due to the presence of bony environment and sustained peptide release. Notably, BP nanosheets in scaffolds significantly reduced the long-term toxicity phenomenon of released DOX during *in vivo* bone regeneration. Our study also provides insights for the design of multi-functional tissue engineering scaffolds for treating other tumor resection-induced tissue defects.

Introduction

Human tissue resection due to tumor, disease or even trauma often causes severe tissue defects and hence tissue or organ dysfunction, greatly lowering patient's life quality. Meanwhile, as tissue defects with a critical-size cannot get healed by themselves, tissue engineering scaffolds are required to enable complete tissue regeneration. Three-dimensional (3D) printing has now gained great attention for applications in treating human tissue defects. By employing appropriate 3D printing techniques (e.g., fused deposition modeling (FDM), selective laser sintering (SLS), ink jetting, micro extrusion with/without post-sintering, etc.), and suitable raw materials (e.g., metals, ceramics, polymers, hydrogels or their composites in forms of wires, powders, pastes or composite solutions), scaffolds with customized shape, tailored pore size/porosity and other desirable features can be fabricated for treating critical-sized human tissue defects.

Towards tumor resection-induced defects[1], as it is difficult to eliminate residual tumor cells completely through surgery interventions solely, subsequent intravenous chemotherapy is required[2]. However, high-dose chemotherapy can result in severe systematic toxicity[3]. To reduce side-effects caused by systemic chemotherapy, 3D printed scaffold containing high-dose chemotherapeutics can be implanted into the defects. Although it was shown that excellent tumor cell elimination and suppression of recurrence at the implantation location could be achieved, the subsequent tissue regeneration was hindered due to the side-effects of locally released high-dose chemotherapeutics[4,5]. Alternatively, photothermotherapy, an effective, noninvasive and low-toxic strategy has gained increasing attention in treating local tumor tissues, through the near infrared (NIR) irradiation-induced hyperthermia. Ma *et al.* produced a bifunctional graphene oxide-modified tricalcium phosphate (GO-TCP) composite scaffold through micro extrusion-based 3D

printing, followed by sintering and post-adsorption of GO[2]. Tumor cells were killed efficiently via photothermotherapy and improved osteogenic differentiation of rabbit bone marrow derived mesenchymal stem cells and bone regeneration *in vivo* were obtained. They also reported a 3D-printed bioceramic scaffold with a uniformly self-assembled calcium phosphate/polydopamine (PDA) nanolayer surface. Improved tumor cell killing via PDA-related photothermotherapy and enhanced bone regeneration were also achieved[6]. Among different types of photothermal agents, single-layered two-dimensional (2D) black phosphorus (BP) nanosheet has been proposed as the most promising nano-sized biomaterial with photothermal effect to treat tumor cells *in vivo*, since BP nanosheets simultaneously possess the following features: (1) strong NIR absorbance and high-photothermal-conversion efficiency; (2) ultrahigh surface area-to-volume ratio for efficient drug loading; (3) favorable biocompatibility and controlled biodegradability and (4) non-toxic and beneficial degradation products for tissue regeneration. In comparison, photothermal materials such as graphene, GO, MoS_2, etc., cannot degrade *in vivo* while PDA has a too high degradation rate (i.e., 40% weight loss within 24 h in PBS), although they all have excellent photothermal effects[6-9]. Yang *et al.* 3D printed and sintered bioglass scaffolds and coated BP nanosheets on the scaffold surface. Prompt photothermotherapy was triggered to kill tumor cells and degradation products of BP nanosheets was found to support bone regeneration[8]. However, the sole use of photothermotherapy to kill residual tumor cells is insufficient as tumor recurrence arising from the residual cells which survived from photothermotherapy could occur. Therefore, better solutions are needed to realize both prompt tumor cell killing and suppression of recurrence with lowered side-effects.

For tissue regeneration, as biomolecules such as growth factors and their functionally equivalent peptides are far more effective than bioactive inorganics and metal salts in inducing cell

differentiation and tissue repair, 3D printed scaffolds with the capability of high-dose biomolecule loading are highly desirable. It is relatively easy to load biomolecules or even cells in hydrogel structures through 3D biorpinting with the assistance of ion/UV crosslinking. However, low mechanical strength, fast biomolecule release and too high degradation rate of 3D printed hydrogel structures restrict their success in long-term tissue regeneration of hard tissues[11-13]. On the contrary, although scaffolds made through fused FDM, SLS and micro extrusion of ceramic pastes followed by sintering have excellent mechanical properties, it is highly difficult to incorporate high-dose thermal-sensitive biomolecules in scaffolds to achieve a sustained release, as these techniques require high temperature processing conditions, which will result in the biological activity of thermal-sensitive drugs/biomolecules being lowered. Thus, surface modification on these scaffolds are needed to enable post-fabrication adsorption of biomolecules with a limited amount and a quick release rate[9,10]. With the above considerations, a facile and versatile strategy is urgently needed to not only enable excellent tumor cell elimination and suppression of tumor recurrence but also improve the tissue regeneration.

In this study, to treat tumor resection-induced tissue defects (in this case, bone tumor resection-induced bony defects were used as a model), hydrophobic BP nanosheets, hydrophilic doxorubicin hydrochloride (DOX) and hydrophilic osteogenic peptide were used as photothermal agent, anti-cancer drug and osteogenic factor, respectively, and were incorporated into water-in-oil composite emulsions comprising of deionized (DI) water, β-tricalcium phosphate (β-TCP) nanoparticles and poly(lactic-co-glycolic acid)/dichloromethane(PLGA/DCM) solutions to form multi-delivery printing inks for the layer-by-layer construction of multifunctional scaffolds through a micro extrusion-based 3D printing in a cryogenic environment. The multi-functional scaffolds had hierarchically porous biomimetic structure, sufficient mechanical strength

(comparable to human cancellous bone), excellent photothermal effect and controlled release of DOX and peptide. By using the multi-functional scaffolds, elimination of tumor cells and long-term prevention of tumor recurrence were achieved in bone tumor-bearing nude mice via on-demand BP-related photothermotherapy and sustained and localized DOX release at a very low concentration *in vitro* and *in vivo*. Subsequently, up-regulated *in vitro* osteogenic differentiation of rat bone marrow derived mesenchymal stem cells (rBMSCs) and greatly enhanced *in vivo* bone regeneration in cranial defects of rats were achieved due to the synergistic effect of bony environment and sustained peptide release, whereas the presence of BP nanosheets in scaffolds significantly reduced the long-term toxicity phenomenon of released DOX during bone regeneration.

Results

Design of multi-functional Scaffolds

The successful fabrication of multi-functional scaffolds relies both on the use of water-in-oil composite emulsion inks, in which BP nanosheets, DOX and P24 peptide were simultaneously delivered, and the micro extrusion-based 3D printing under a cryogenic environment. To formulate the inks, BP nanosheets and TCP microparticles were homogeneously distributed in PLGA/DCM solutions (oil phase) via ultra-sonication, while P24 peptide and DOX were dissolved in the aqueous solution containing collagen I (water phase), followed by a mixing of the water phase with the oil phase in a specific sequence (**Fig.1a**). The as-formulated inks were then subjected to a micro-extrusion based cryogenic 3D printing to obtain customized multi-functional scaffolds. Our multi-functional scaffolds were designed to kill the tumor cells *in vitro* and *in vivo* through the on-demand BP-related photothermotherapy and suppress the tumor recurrence via the sustained-localized DOX release, whereas the *in vitro* rBMSC osteogenic

differentiation and *in vivo* bone regeneration were achieved afterwards via the synergistic effects of controlled delivery of P24 peptide and β-TCP presence (**Fig.1b**). The multi-functional DOX/P24/BP/TCP/PLGA scaffold was designated as "BDPTP" scaffolds, while BP/P24/TCP/PLGA, DOX/P24/TCP/PLGA, P24/TCP/PLGA and TCP/PLGA scaffolds were designated as 'BPTP', 'DPTP', 'PTP' and 'TP' scaffolds, respectively.

Characterization of multi-functional Scaffolds

Cryogenic 3D printing enabled the fabrication of multi-functional scaffolds with a patterned structure, which was structurally identical to the CAD model. As shown in **Fig.2a**, patterned TP and PTP scaffolds had a white color. The incorporation of 4.5 mg of BP nanosheets in 3 g of BPTP scaffolds resulted in a gray color. The BP nanosheets had a diameter of 50 to 150 nm and an average thickness of 8 nm (**Figure.S1**). The incorporation of 0.166 mg of DOX in 3 g of scaffolds changed the color of DPTP scaffolds into light pink, whereas BDPTP scaffolds showed a dusty pink color. All scaffolds had a 13-layer structure with an overall thickness of 3 mm and each layer consisted of 18 paralleled rods with a length of 14 mm and a diameter of 0.35 mm. Rods in adjacent layers had a cross angle of 90 °, hence forming square holes with a side length of 360 ± 40 μm (**Fig.2b**). The cross-sections of these scaffolds were also identical to that of the CAD model, indicating that excellent fabrication accuracy could be achieved during cryogenic 3D printing (**Fig.2c**). The BDPTP scaffolds and other controls had a rough strut surface on which elliptical micropores with a relatively high alignment were observed, hence exhibiting a hierarchically porous structure (**Fig.2b**). A large number of β-TCP particles with a diameter less than 200 nm appeared on the strut surface and also the porous cross-section of the strut matrix, showing a homogeneous distribution in multi-functional scaffolds and respective control scaffolds.

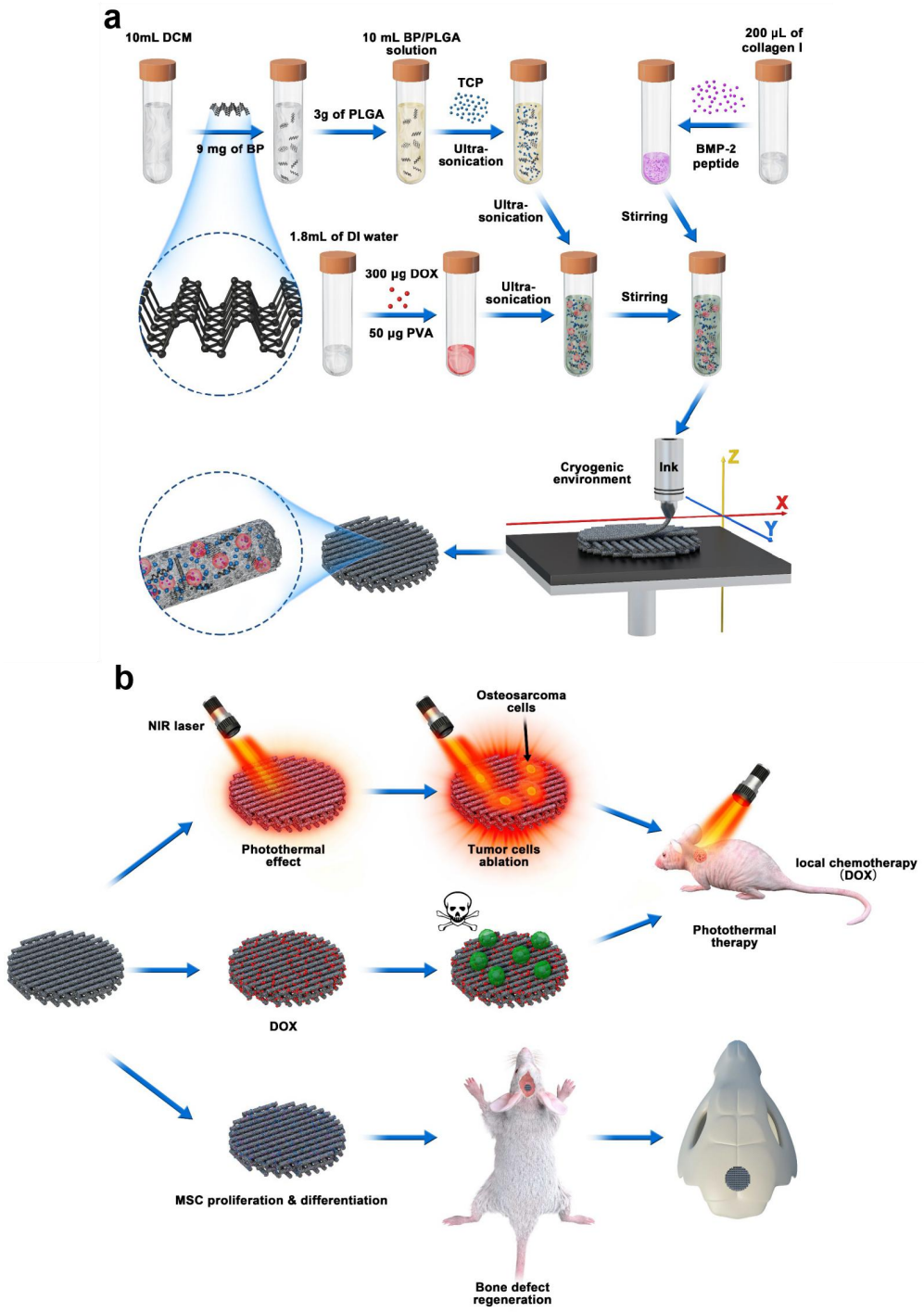

Figure.1 Schematic illustration of cryogenic 3D printing of multi-functional scaffolds and their multi- functions. (a) formulation of multi-delivery inks and 3D printing of multi-functional scaffolds; (b) tumor tissue ablation in nude mice through photothermal therapy and localized chemotherapy and regeneration of cranial bone defects of rats implanted with multi-functional scaffolds.

In addition, collagen I nanofibers with a diameter of 200 nm were found on the strut surface as well (**Fig.2b** and **c**). Through the elemental mapping examination, Ca and P elements were found to uniformly distribute on scaffold surface (**Fig.2d**), which were further verified by the EDX spectrum (**Fig.2e**). Besides, it was found that the addition of BP nanosheets changed the atomic ratio of Ca and P in scaffolds from 1.50 (e.g., PTP scaffolds) to 1.48 (BDPTP scaffolds). The mechanical properties of BDPTP scaffolds and other controls were investigated through compression testing. All scaffolds immersed in PBS had a compressive strength and an elastic modulus of 4-4.5 MPa and 12.2-14.6 MPa at 37 ^{o}C, respectively, which were comparable to human cancellous bone at the physiological condition, suggesting that our scaffolds were mechanically capable of repairing defected human cancellous bone (**Fig.S2a**). The degradation of BDPTP scaffolds and other controls was monitored in an 8-week test period. With increasing incubation time, all scaffolds showed a continuously decreased weight remaining and achieved about 13-18% weight loss after 12-week incubation (**Fig.S2b**). The macroscopic structure of all scaffolds after 12-week degradation *in vitro* was well maintained comparing to that without degradation tests (**Fig.S2c**).

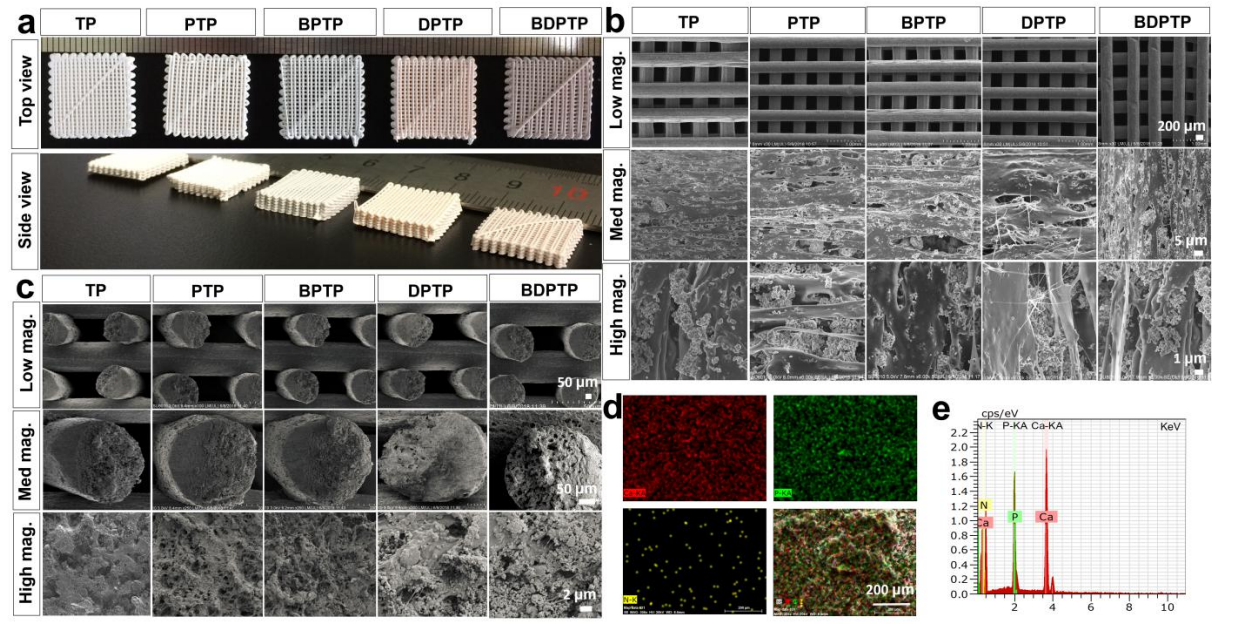

Figure.2 Structure, morphology and elemental analysis of cryogenic 3D printed scaffolds. (a) macroscopic morphology of different scaffolds captured using digital camera; (b) SEM micrographs of different scaffolds with low, medium and high magnifications (top view); (c) SEM micrographs of different scaffolds with low, medium and high magnifications (cross-section); (d) EDX elemental mapping of Ca, P, N on the surface of BDPTP scaffolds; (e) EDX spectrum of Ca, P, and N on the surface of BDPTP scaffolds.

In Vitro and *In Vivo* Tumor Ablation Through Photothermo-chemotherapy

In this study, BP nanosheet was used as a desirable photothermal agent to provide scaffolds with excellent photothermal performance, and hence to kill tumor cells via hyperthermia. BDPTP and BPTP scaffolds adsorbed with PBS showed excellent photothermal effects when 808 nm irradiation was applied. By changing the power density of laser from 0.5 to 2.0 W cm^{-2}, the temperature of the scaffolds was increased from room temperature to 60 °C within 10 min (**Fig.3a**). Upon NIR with a certain power density, the temperature of BDPTP and BPTP scaffolds increased rapidly in a short time period, and then maintained at a stable temperature as irradiation time increasing because of the heat balance between production and dissipation (**Fig.3b**). In comparison, TP, PTP and DPTP scaffolds had no photothermal effect under NIR

irradiation. The temperature distribution of different scaffolds after 10 min NIR irradiation is shown in **Fig.3c**. No temperature increase was detected on TP, PTP and DPTP scaffolds, whereas significantly higher temperature was detected for BPTP and BDPTP scaffolds. As the laser energy density of the center site was slightly higher, the center site of the scaffolds showed a white color and achieved 50 ^{o}C. Different from other studies which deposited BP nanosheets on scaffolds surface to provide a short-term photothermal effect due to the instability of BP nanosheets, our BDPTP and BPTP scaffolds maintained the photothermal ability for up to 4 weeks, although the highest photothermal temperature was reduced from 60 ^{o}C at week 0 to 37 ^{o}C at week 4 (**Fig.3d**). The *in vitro* release behavior of DOX from BDPTP and DPTP scaffolds, with a 10 min of NIR irradiation at the beginning was investigated in a 14-day period (**Fig.S3a**). DOX released from DPTP scaffolds had a moderate level of initial burst release in 24 h (6.5 ± 1.5 % level), followed by a slow but steady release up to 26 ± 2% level in 14 days with or without NIR irradiation. Slightly lowered DOX release was obtained for BDPTP group due to the presence of BP in scaffolds, which showed a 23 ± 2% total release level in 14-day period. In comparison, the DOX released from BDPTP scaffolds had an accelerated release behavior when 10 min of NIR irradiation was applied at the beginning of release tests, showing a 2-fold instantaneous release up to 11 ± 1.8 % level within 24 h. This could be attributed to the faster diffusion of DOX into the test liquid at a higher temperature. Likewise, when the NIR irradiation was applied daily, a pulsed DOX release was detected and this further increased the total release amount of DOX in 14-day test epriod (**Fig.S3b**). **Fig.3e** shows the viability of MG63 cells cultured on scaffolds for 1, 4 and 7 days without NIR irradiation. Cell proliferation was observed on all scaffolds with increasing culture time and PTP and BPTP scaffolds induced the highest cell proliferation, whereas DPTP and BDPTP scaffolds were found to delay the cell proliferation

as the released DOX could cause cell apoptosis gradually. When NIR irradiation was applied on cell-scaffold constructs for 5 min, nearly all MG63 cells on BPTP and BDPTP scaffolds were killed (color in red) after 1-day culture, whereas no cell death was observed on PTP scaffolds. In comparison, less living cells were observed on DPTP scaffolds and this trend was verified by CCK8 assay 1 day after NIR irradiation (**Fig.3f** and **g**). In this study, tumor-bearing nude mice model was used as animal models to investigate the anti-cancer performance of scaffolds. **Fig.3h** shows the temperature distribution of tumor tissues embedded with scaffolds under NIR irradiation. Obvious temperature increase was tracked in BPTP and BDPTP groups under NIR irradiation, whereas no significant temperature increase was observed for TP, PTP and DPTP groups (**Fig.3i**). After 10 min of NIR irradiation treatment, the body weight and tumor volume of the nude mice was monitored up to 16 days (**Fig.S4** and **Fig.3j**). The digital images of typical tumor tissues collected from mice implanted with different scaffolds after 16 days is shown in **Fig.3k**. Without NIR irradiation treatment, the tumor size increased with increasing feeding time. Comparing TP, PTP and BPTP groups, tumor tissues in DPTP and BDPTP groups had a smaller size (p <0.05). In comparison, upon NIR irradiation, BDPTP and BPTP scaffolds induced obvious tumor ablation, showing significantly reduced tumor volume from 200 to 0 mm^3 at day 4. However, severe tumor recurrence was observed for the BPTP group which reached a tumor volume over 200 mm^3 at day 16. In comparison, a significantly lowered tumor recurrence rate with a significantly smaller tumor volume was obtained for the BDPTP groups, suggesting our scaffolds with both photothermotherapy and chemotherapy capabilities had a synergistic effect on *in vivo* tumor elimination, in which the survived tumor cells undergone photothermotherapy could be further killed by sustained-localized DOX release at a low concentration.

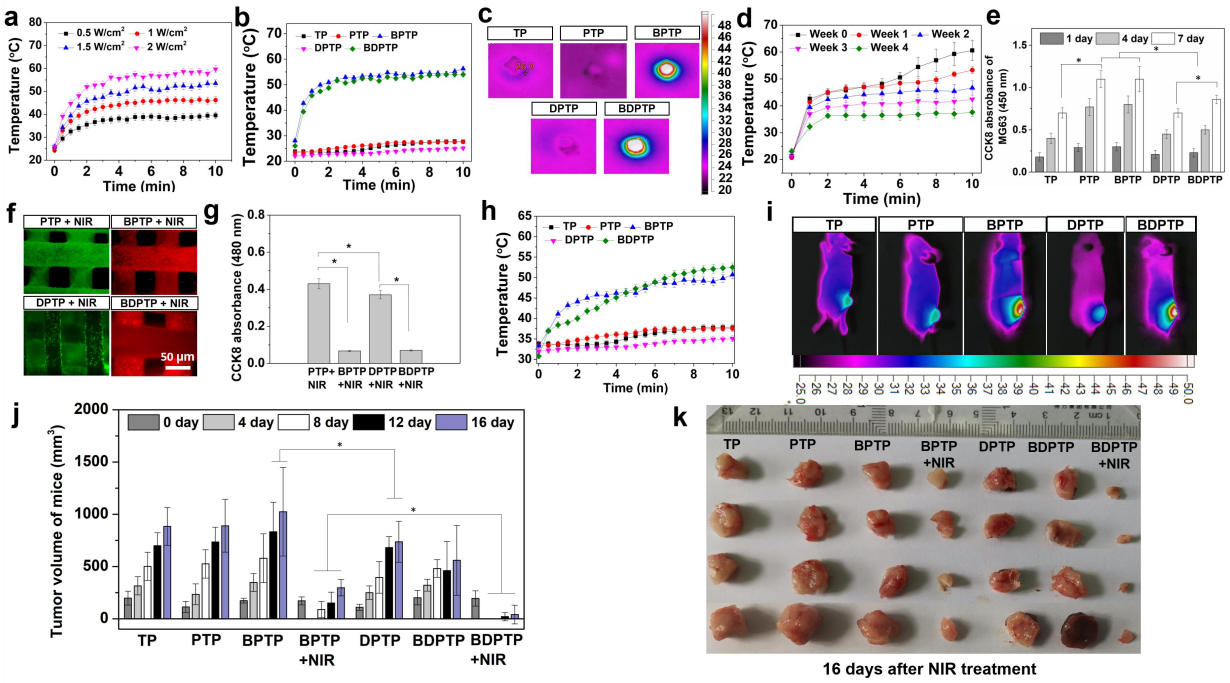

Figure.3 *In vitro* and *in vivo* ablation of tumor cells with the treatment of photothermal therapy and/or chemotherapy. (a) effect of NIR laser power on the temperature increase of BDPTP scaffolds; (b) effect of temperature increase of different scaffolds irradiated by NIR laser; (c) temperature distribution of scaffolds treated with NIR laser; (d) Temperature increase of BDPTP scaffolds under NIR irradiation with increasing culture time; (e) MG63 cell proliferation with increasing culture time; (f) live and dead images of cells on different scaffolds 1 day after 10 min of NIR irradiation; (g) viability of cells on different scaffolds treated with 10 min of NIR laser; (h) temperature increase of tumor tissues implanted with different scaffolds upon 10 min of NIR laser irradiation *in vivo*; (i) temperature distribution of tumor tissue implanted with scaffolds *in vivo*; (j) volume of tumors in nude mice after treatment; (k) digital images of typical tumor tissues collected from nude mice of each group at day 16 with/without NIR irradiation. For panels a, b, d, e and g, n = 4. For panels j and k, n = 4, $*p < 0.05$ by one-way ANOVA test. All error bars indicate mean ± standard deviation.

In Vitro rBMSC Osteogenic Differentiation and *In Vivo* Rat Cranial Bone Regeneration

After studying the anti-cancer performance, the bone regeneration capability of multi-functional scaffolds was studied by evaluating the biological performance of scaffolds *in vitro* and regeneration of critical-sized rat cranial defects *in vivo*. The *in vitro* release behavior of osteogenic peptide is shown in **Fig.S5**. P24 peptide released from all scaffolds showed a similar profile, consisting of an initial burst release, followed by a slower but more steady release.

Among all groups, peptide released from DPTP scaffolds exhibited a gradually accelerated release behavior, showing the highest total release level in 24 days. This could be attributed to the accelerated P24 diffusion through the pores made during the DOX release. In comparison, due to the presence of BP nanosheets, the release of P24 peptide from BPTP and BDPTP scaffolds was slower than that released from PTP and DPTP scaffolds, in which BPTP scaffolds exhibited the lowest total release level. When a 10 min of NIR irradiation was applied daily in initial 4 days, the peptide released from BPTP and BDPTP scaffolds was 1.5-fold of that without NIR irradiation, and the total release level was also increased in first 5-day period, suggesting the temperature increase in scaffolds could accelerate the P24 peptide release.

To follow our design that the scaffolds were firstly used for tumor cell elimination and then for inducing bone regeneration, all scaffolds immersed in PBS were NIR irradiated for 10 min and immersed in PBS for 1 day, followed by the transfer of scaffolds to a new culture plate for rBMSC seeding and cranial implantation (**Figure.S6**). Nearly all rBMSCs on PTP, BPTP, DPTP and BDPTP scaffolds were alive (color in green) and a few dead cells (color in red) were found on DPTP scaffolds after 3 days of culture (**Fig.4a** and **b**). The proliferation of rBMSCs on scaffolds was also monitored in a 14-day period and similar trend was obtained, in which PTP, BPTP and BDPTP scaffolds induced significantly higher cell proliferation level than TP and DPTP scaffolds ($p < 0.05$) (**Fig.4c**). After 1 day culture, a number of F-actin filaments (color in green) and vinculin adhesive plaques (color in red) which were located around the nucleus (color in blue) were observed in rBMSCs cultured on different scaffolds via confocal laser scanning microscopy (CLSM), indicating that the strut surface of multi-functional scaffolds as well as other controls were favorable for initial cell adhesion, in which the vinculin dot density on PTP, BPTP and BDPTP scaffolds was significantly higher than that on TP and DPTP scaffolds

(**Fig.4d**). After 7-day culture, numerous rBMSCs were observed on all scaffolds and showed an expanded morphology, indicating these hierarchically porous scaffolds were favorable microenvironments for cell spreading (**Fig.4d**). All these results demonstrate that the incorporation of TCP microparticles in scaffolds could support the adhesion, proliferation and maturation of rBMSCs and the *in situ* delivery of P24 peptide could further improve rBMSC growth. As the temperature of the multi-functional scaffolds could increase to about 50 ^{o}C to kill tumor cells under NIR irradiation, whether P24 peptide could maintain its biological activity at such a temperature is concerned. As shown in **Fig.S7a** and **b**, after 7 and 21-day culture, PTP scaffolds treated at 45 ^{o}C for up to 30 min induced similar level of alkaline phosphatase (ALP) activity and cell mineralization comparing to that treated at 37 ^{o}C, suggesting the P24 peptide could maintain its stability at a relatively high level after short-term photothermal treatment. When the peptide solution was treated at 50 ^{o}C for 10 to 30 min, disernable reduction of rBMSC osteogenic differentiation and mineralization was detected comparing to that treated at 37 ^{o}C, but still significantly higher than control group. The effects of scaffolds on osteogenic differentiation of rBMSCs was then investigated. After 7 and 14 days of culture, extracts of PTP, BPTP, DPTP and BDPTP scaffolds induced similar level of ALP expression (color in violet), which was stronger than that induced by TP scaffolds (**Fig.4e**). This was confirmed by the ALP activity assay, in which rBMSCs on PTP and BPTP scaffolds exhibited the highest ALP activity at day 7 and 14 ($p < 0.05$) (**Fig.4f**). Likewise, significantly larger calcium deposition area was observed in rBMSCs cultured with extracts of PTP, BPTP and BDPTP scaffolds (**Fig.4e**), which was further verified by the absorbance of dissolved red calcium nodules (**Fig.4g**).

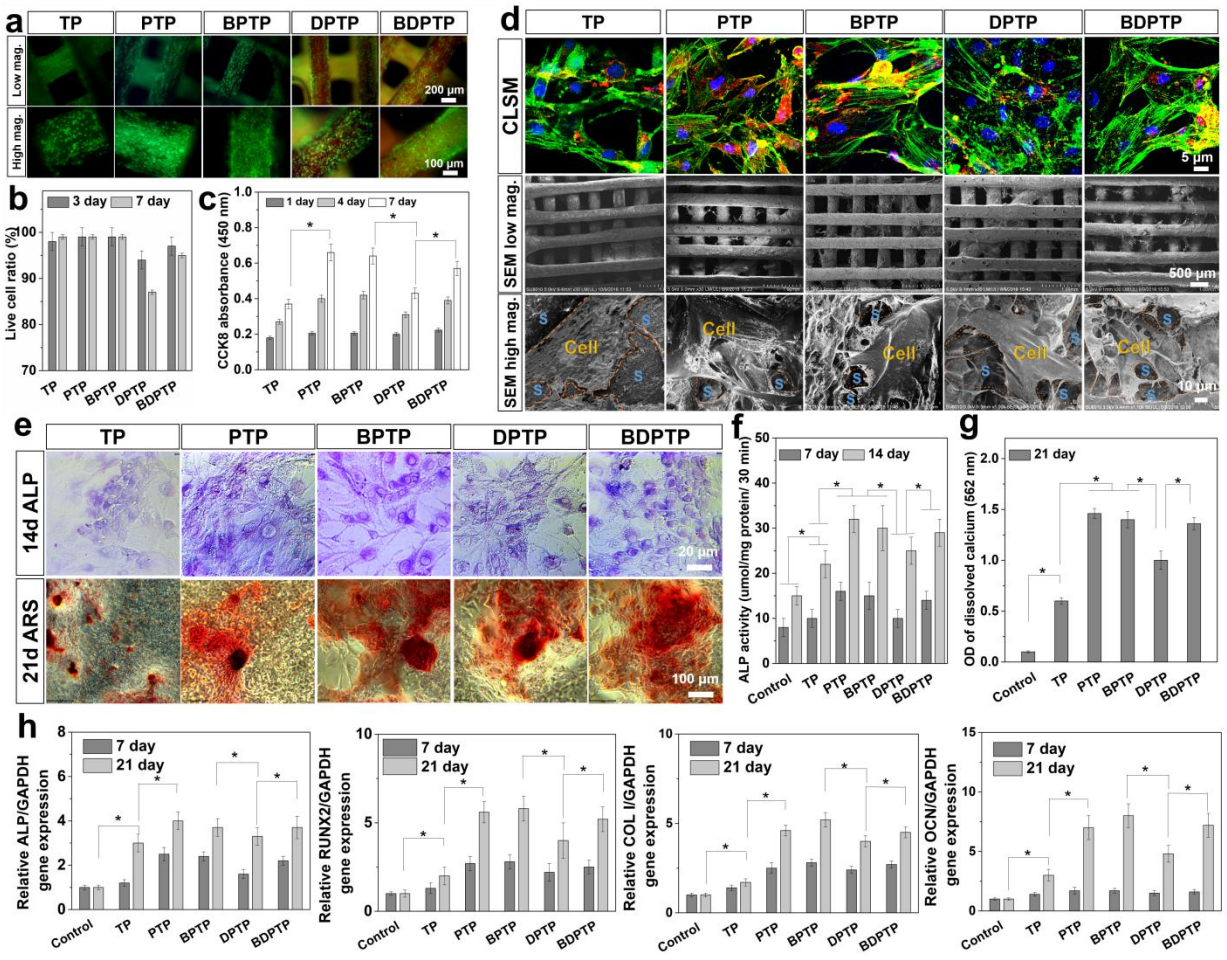

Figure.4 *In vitro* growth and osteogenic differentiation of rBMSCs. (a) live and dead images of rBMSCs cultured on different scaffolds for 3 days; (b) viability of rBMSCs at day 3 and 7; (c) proliferation of rBMSCs on scaffolds in a 7 days; (d) expression of vinculin adhesive plaques and F-actin cytoskeleton of rBMSCs on scaffolds in 24 h and cell morphology on scaffolds after 7-day culture; (e) alkaline phosphatase (ALP) staining of alizarin red S (ARS) staining of rBSMCs cultured with extracts of different scaffolds; (f) ALP activity of rBMSCs cultured on scaffolds for up to 14 days; (g) absorbance of dissolved ARS staining nodules at 562 nm; (h) gene expression of ALP, RUNX2, collagen I (COL I) and osteocalcin (OCN) in rBMSCs cultured on scaffolds for up to 21 days. For panels b, c, f, g and h, n = 4, $*p < 0.05$ by one-way ANOVA test. All error bars indicate mean ± standard deviation.

The osteogenic gene expression of rBMSCs cultured on scaffolds were studied using quantitative real-time polymerase chain reaction (qPCR). After 7-day culture, TP scaffolds up-regulated the gene expression of RUNX2, ALP and COL I than the control group, whereas P24 peptide containing scaffolds induced significantly higher gene expression than TP scaffolds, suggesting P24 peptide was the dominant factor in induce the early osteogenic differentiation (**Fig.4h**).

After 21-day culture, the expression level of RUNX2, ALP, COL I and OCN was increased for all groups, in which the expression level of OCN in PTP, BPTP and BDPTP groups achieved a 3.2 to 3.7-fold increase compared to that at day 7, whereas the TP group only showed a 1-fold increase, suggesting the continuous release of P24 peptide could constantly stimulate osteogenic differentiation of rBMSCs, especially at the late stage. These results demonstrated that multi-functional scaffolds enhanced the hBMSCs growth and up-regulated the osteogenic differentiation *in vitro*.

Circular defects with a diameter of 5 mm were created on cranial bone tissue of rats to establish animal model with a critically-sized bone defects and scaffolds with matched size and thickness were implanted to study the *in vivo* bone regeneration for up to 3 months (n=5 for each group) (**Fig.5a** and **b**). 2 months after surgery, the control group had very limited new bone formation, whereas TP scaffolds slightly up-regulated the new bone formation at the peripheral part of the incision defects, suggesting TP scaffolds had excellent osteoconductivity (**Fig.5c**). In contrast, significantly higher volume of new bone formation was observed at the central part of the defected area when BPTP and DPTP scaffolds were implanted, while much more new bone regeneration was observed in defects implanted with PTP and BDPTP scaffolds. 3 months after surgery, uniform new bone formation at the central part of the defects was significantly up-regulated for PTP, BPTP and BDPTP groups, whereas DPTP and TP scaffolds induced much less new bone formation. **Fig.5d** shows the bone volume/total volume (BV/TV) ratio of each group. 45 ± 8, 40 ± 7 and 38 ± 5% new bone formation was achieved for PTP, BPTP and BDPTP scaffolds after 3 months, respectively, whereas only 15 ± 4, 21 ± 4 and 25 ± 4% new bone formation were induced by negative control, TP and DPTP scaffolds, respectively. **Fig.5e** shows the bone mineral density (BMD) of different groups. Likewise, the BMD value of PTP,

BPTP and BDPTP groups was significantly higher than negative control, TP and DPTP groups ((423 ± 60, 400 ± 50 and 385 ± 50 vs. 57.5 ± 29, 143 ± 41 and 270 ± 40 mg/mm^3), ($p < 0.05$).

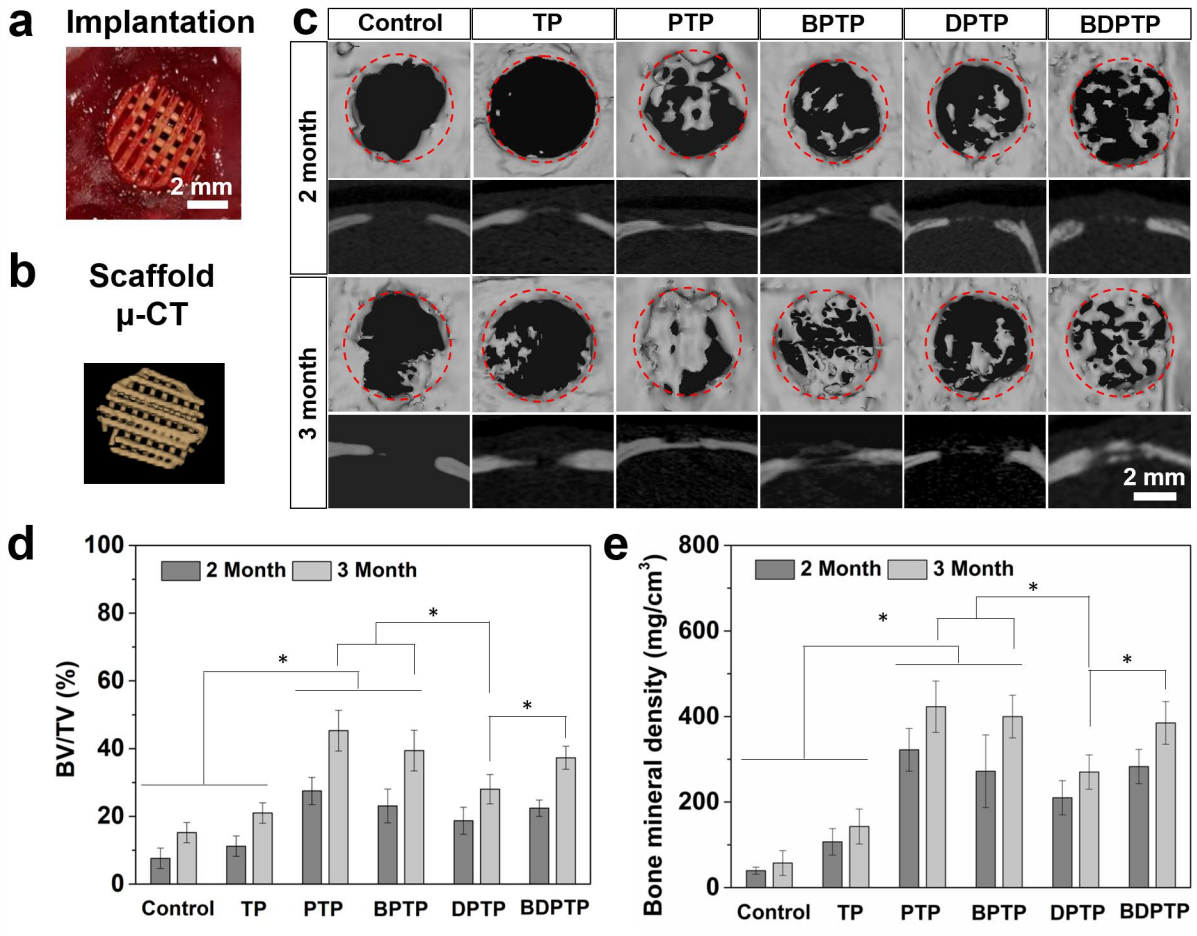

Figure.5 *In vivo* bone regeneration in cranial bone defects of rats. (a) implantation of scaffolds; (b) micro-CT image of implanted scaffolds; (c) micro-CT images of cranial defects implanted with different scaffolds for 2 and 3 month, respectively; (d) bone volume/total volume (BV/TV) of regenerated tissue in rat cranial defects (the volume of scaffold was subtracted already); (e) bone mineral density of tissues regenerated in rat cranial defects. For panels d and e, n = 5, *$p < 0.05$ by one-way ANOVA test. All error bars indicate mean ± standard deviation.

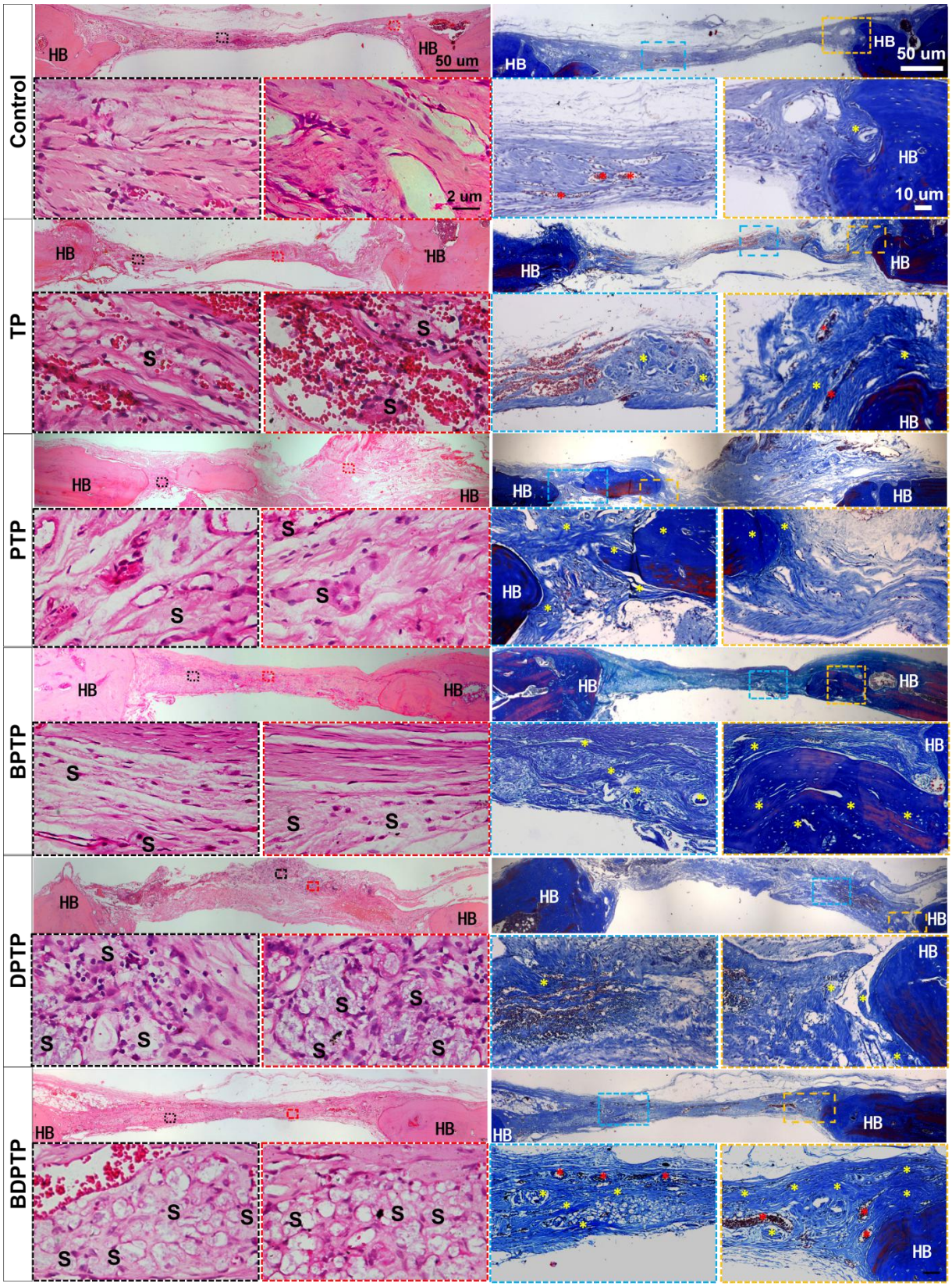
Control
TP
PTP
BPTP
DPTP
BDPTP
HB
S
50 um
2 um
10 um

Figure.6 Histological analysis of regenerated tissues in the rat cranial defects 3 month after the implantation of different scaffolds through H&E staining and Masson's trichrome staining. Micrographs with a low magnification show the sectioned slice of entire cranial defect region. H&E micrographs with a high magnification show the representative images of scaffolds embedded in regenerated tissues at different regions. Masson's micrographs with a high magnification show the representative images of the edge and central area of the defects. Notes: "S" represents scaffold; "HB" represents host bone; "yellow star" indicates the new bone and osteoid and "red star" represents newly formed capillary vessel.

The H&E staining and Masson's trichrome staining were subsequently conducted to examine the tissues regenerated in each group (**Fig.6**). Scaffolds fragments (labeled with 'S') could be observed in all groups except negative control group. Similar to the results obtained from micro-CT data, the histological examination revealed variable amounts of new bone formation in different groups. Tissues regenerated in TP and negative control groups had the lowest thickness and only very limited new bone formation was observed at the peripheral part of the defects, whereas a large amount of fibrous tissues as well as some capillary vessels (labeled with red stars) were observed at the central part of defects. In comparison, significantly more mineralization centers (labeled with yellow stars) were found in DPTP group and much more new bone and bone trabecula structure (labeled with yellow stars) were observed in PTP, BPTP DPTP and BDPTP groups (i.e., dark blue area). The regenerated new bone tissue in BDPTP group exhibited a sandwich-like structure, in which more capillary vessels were observed, suggesting our multi-functional scaffolds were favorable platforms for inducing bone regeneration.

Discussion

So far, the mostly employed clinical strategy to treat solid tumor is to remove tumor tissue through surgery, followed by the elimination of residual tumor cells via intravenous chemotherapy[15]. However, as several types of tumor cells are not sensitive to the existing chemotherapeutics, patients suffer from not only low specificity/efficiency of the intravenous

chemotherapy and bad prevention of tumor recurrence but also strong side-effect on tissues and organs[16-18]. Moreover, the tumor resection-induced defects with a critical size normally cannot get healed by themselves[19,20], hence developing a versatile strategy to realize both residual tumor removal/prevention of tumor recurrence and regeneration of tissues with a critical size and customized shape is of great importance and still challenging. In this study, a facile strategy based on cryogenic 3D printing of multi-delivery emulsion inks was designed to produce multi-functional (i.e., functions including tumor elimination, recurrence suppression and tissue regeneration) scaffolds with customized shape, adjustable macro/microporous structure and controlled mechanical strength for treating tumor resection-induced tissue defects. Biodegradable polyesters, hydrophobic photothermal agents can be dissolved or dispersed in organic solvents (regard as "oil phase") of emulsion inks while hydrophilic chemotherapeutics and functional biomolecules can be dissolved in the aqueous solution (regard as "water phase") of emulsion inks. When a lower polymer concentration or a higher aqueous phase volume was used to formulate emulsion inks, scaffolds with a lower density, a larger pore size, a lower compressive strength and a faster drug/biomolecule release can be produced to treat soft tissue tumor resection-induced defects. On the contrary, if the polymer concentration is high and a large amount of bioceramics were imparted, scaffolds with a significantly higher compressive strength and improved osteoconductivity can be made to treat bone tumor resection-induced defects. For instance, in this study, TCP/PLGA nanocomposite emulsions loaded with BP nanosheet, DOX hydrochloride and P24 peptide (i.e., a peptide functionally equivalent to bone morphogeneic protein-2), were used as printing inks to produce multi-functional scaffolds to treat bone tumor resection-induced bone defects. It is worth noting that compared to sintered bioceramic scaffolds which further immobilized functional agents through the surface deposition/adsorption, our

strategy is superior in *in situ* incorporation of multiple bio-agents with uniform distribution, high initial loading level and controlled release profile while sufficient mechanical strength, adjustable macro-micro hierarchically porous structure, etc. could still be maintained [2,6,8]. Excellent anti-cancer performance comprising of prompt tumor cell elimination and long-term recurrence suppression could be achieved by on-demand photothermotherapy and localized-sustained release of low-dose chemotherapy whereas improved bone regeneration could be achieved afterwards due to the sustained release of osteogenic peptide from a bony environment (i.e., the multi-functional scaffolds contained a large amount of TCP nanoparticles) with sufficient mechanical strength, favorable cellular responses and limited side-effects (e.g., only limited DOX hydrochloride was released at the "regeneration stage")[21, 22].

By adjusting parameters of NIR laser, precise control of the scaffold temperature could be achieved, and the *in vitro* DOX release could be significantly accelerated right after NIR irradiation to rapidly provide the local environment with a therapeutic concentration. Interestingly, our scaffolds could maintain photothermal-conversion ability for more than 3 weeks due to the reduced decomposition rate of BP nanosheets as a large portion of BP nanosheets were embedded in the polymer matrix and only degrades along with PLGA hydrolysis, showing much longer manipulation time window for photothermotherapy than other studies which only deposited BP nanosheets on the scaffold surface[8]. The *in vitro* results indicated that on-demand photothermotherapy was capable of killing tumor cells quickly whereas localized chemotherapy at a low concentration (i.e., 250 nM, 10 mg of scaffolds were immersed 0.5 mL of culture medium for cell culture) was capable of killing bone tumor cells gradually[23]. This was further verified by the *in vivo* results, in which BP-containing scaffolds with 10 min of NIR irradiation induced nearly 100% tumor ablation within 4 days[6]. However,

tumor recurrence was found in BPTP+NIR group whereas tumors with a much smaller size ($p < 0.05$) was found in BDPTP+NIR group after 12 days, indicating photothermotherapy alone is insufficient to eliminate residual tumor cells while the sustained DOX release, even at a low concentration, is favorable for recurrence suppression[24].

Our results showed that PTP scaffolds heated to 45 ^{o}C for up to 30 min in aqueous solution induced similar level of ALP expression and cell mineralization than that at 37 ^{o}C, indicating that photothermal stimulation up to 45 ^{o}C would be safe for maintaining the osteogenic potent of P24 peptide[25,26]. However, too high targeting photothermal temperature (i.e., 50 ^{o}C) with too long single duration of NIR irradiation (e.g., 20 min) which lowered the effectiveness of the osteogenic peptide should be avoided. Different from other studies which adsorbed or conjugated biomacromolecules onto the surface of scaffolds to achieve a short-term release[27-29], as high as 266 μg of P24 peptide was uniformly distributed in 100 mg of multi-functional scaffolds. The peptide release could be attributed to the dissolution of P24 peptide attached/adsorbed to the surface of micropores and the PLGA hydrolysis/erosion induced diffusion of P24 peptide. The slower peptide release from BDPTP and BPTP scaffolds compared to PTP scaffolds could be attributed to the strong non-specific/physical adsorption of peptide onto BP nanosheets which have ultrahigh surface area-to-volume ratio. However, when NIR irradiation was applied, the peptide release from BP-containing scaffolds was significantly accelerated on the contrary, due to the faster diffusion of P24 peptide from scaffolds with a higher temperature. After photothermotherapy (**Figure.S6**), PTP, BPTP and BDPTP scaffolds not only supported the adhesion and proliferation of seeded rBMSCs but also significantly up-regulated osteogenic differentiation of rBMSCs including the gene expression of RUNX2, ALP, COL I and OCN ($p < 0.05$). These results suggest that even a part of P24 peptide could be released during the

photothermotherapy stage, the sustained release of the rest P24 peptide still had sufficient potent to induce bone formation *in vitro* and *in vivo*. Moreover, the supplement of 0.15 mg of BP nanosheets in 100 mg of TCP/PLGA scaffolds (1500 ppm) showed no side-effect on the proliferation, osteogenic differentiation and mineralization of rBMSCs, and BP nanosheets exposed to the culture medium or body fluid could gradually degrade into phosphates, hence providing more salts to participate in cell mineralization[30-32]. In addition, discernable inhibitory effect on the *in vitro* viability, adhesion and proliferation of rBMSCs was observed for DPTP group due to the DOX release even at a low concentration. In comparison, BDPTP scaffolds showed significantly lowered side-effects on rBMSC growth and osteogenic differentiation than DPTP scaffolds ($p < 0.05$), indicating that a more sustained DOX release at the bone regeneration stage due to presence of BP nanosheets was more favorable for *in vitro* growth and osteogenic differentiation of rBMSCs[33]. The *in vivo* animal study also confirmed this trend. The μ-CT images, BV/TV value and BMD value indicated that PTP, BPTP and BDPTP scaffolds induced significantly higher volume of new bone formation that TP and negative control groups ($p < 0.05$), suggesting the controlled delivery of P24 peptide could intensively improve the new bone formation. The reduced bone regeneration volume in DPTP group indicated that the delivery of DOX had discernable long-term inhibitory effect on *in vivo* bone regeneration. Thus, the improved *in vivo* bone forming ability of BDPTP scaffolds comparing to DPTP scaffolds could be attributed to follows: (1) the lowered DOX release due to the non-specific/physical adsorption of DOX onto BP nanosheets and (2) the more sustained peptide release from BDPTP scaffolds than from DPTP scaffolds, which supported the uniform bone formation during the third month. H&E staining and Masson's trichome staining also indicate that tissues regenerated in BDPTP, and also by PTP and BPTP groups, had a significantly higher portion of new bone

tissue, rather than fibrous tissue, compared to that regenerated by control, TP and DPTP groups, showing obvious trabecular structure with obvious osteoids and capillary vessels[34-36]. Besides the excellent biological performance *in vitro* and *in vivo*, our scaffolds had appropriate degradation rate, which is desirable to match the regeneration rate of human bone tissue[37,38]. Apart from the excellent phototheramotherapy, BP nanosheets were also reported to have distinct bioactive phosphorus-based chemotherapy. Therefore, the role of BP nanosheets in anti-cancer therapy via combined photothermotherapy and chemotherapy could be elucidated in future[39].

In summary, by using multi-delivery water-in-oil composite emulsions as printing inks, hierarchically porous and mechanically strong multi-functional scaffolds were successfully fabricated through cryogenic 3D printing. Excellent tumor cell ablation *in vitro* and *in vivo* was achieved via the efficient photothermotherapy and by a sustained and localized chemotherapy, while significantly improved rBMSC osteogenic differentiation *in vitro* and enhanced regeneration of the defected rat cranial bone *in vivo* were also realized. Notably, the long-term inhibitory effect of DOX release on bone regeneration was significantly reduced. This study provided a facile and versatile method to produce multi-functional scaffolds with required structure, mechanical strength, anti-cancer capability and regeneration ability for treating tumor resection-induced tissue defects.

Experimental Procedures

Materials

Poly(D,L-lactic-*co*-glycolic acid) (PLGA) with an inherent viscosity of 0.8 dL/g was provided by Jinan Daigang Biotechnology Limited, Shandong, China. β-tricalcium phosphates (β-TCP) with an average diameter of less than 0.2 μm and dichloromethane (DCM) were Shanghai Aladdin

LTD products. Black phosphorus (BP) nanosheets were produced in our lab [7]. Bone morphogenetic protein-2-like osteogenic peptide (P24) with a sequence of KIPKA SSVPT ELSAI STLYL SGGC and a purity of 98.12% was synthesized by Shanghai Ziyu Biotechnology LTD, China. Collagen type I (from rat tail) was supplied by Corning, Inc. DOX was a Sigma-Aldrich product (USA). DI water for all experiments was obtained using a DI water producer (Model D12681, Barnstead International, USA). Tween 20, phosphate buffered saline (PBS) tablets and bovine serum albumin (BSA) were Sigma-Aldrich products (USA).

Formation of DOX/BP/P24/TCP/PLGA water/oil composite emulsion inks

330 μg of DOX and 50 μL of Tween 20 were firstly dissolved in 1.5 mL of DI water and were blended with 10 mL of BP/TCP/PLGA/DCM composite polymer suspensions, in which 9 mg of BP nanosheets were suspended in 10 mL of DCM through 30 min ultra-sonication, followed by the dissolution of 3 g of PLGA and the addition of 3 g of TCP microspheres, with the assistance of 10 min ultra-sonication. Afterwards, the mixture of 200 μL of collagen I solution (9.5 mg/mL), 10.6 μL of 1N NaOH and 8 mg of P24 peptide was added into the as-prepared composite emulsions for a 10 min manual mixing at 100 rpm, forming printing inks. The as-printed DOX/P24/BP/TCP/PLGA scaffolds were designated as “BDPTP”. Similarly, other inks with the incorporation of fewer types of biologically active agents were also made as controls, in which BP/P24/TCP/PLGA scaffolds, DOX/P24/TCP/PLGA scaffolds, P24/TCP/PLGA scaffolds and TCP/PLGA scaffolds were designated as “BPTP”, “DPTP”, “PTP” and “TP”, respectively.

Fabrication of BDPTP scaffolds through cryogenic 3D printing

BDPTP inks were firstly loaded in a 20 mL syringe connected with a plastic V-shape nozzle (inner diameter: 0.4 mm) and then inserted into the locator of printing machine in which the

syringe piston could be pumped by the programmed screw extruder. After adjusting the environmental temperature to -10 ~ -30 ^{o}C, a pre-designed CAD model (i.e., each scaffold had a 12-layer structure and each layer consisted of 19 paralleled rods with a length of 14 mm and a diameter of 0.4 mm; rods in adjacent layers had a cross angle of 90 ^{o}) was then opened in the printing software to print BDPTP scaffolds layer-by-layer. A fan was placed on the stage to provide continuous flow to remove DCM from the as-extruded patterns. After the model construction, the cryogenic air drying was maintained for 1 h to remove residual DCM.

Scaffold characterization

The structure and morphology of BP nanosheets were studied using atomic force microscopy and transmission electron microscopy. The macro- and microscopic morphology of 3D printed scaffolds was observed using digital camera and SEM (Leo 1530 Gemini, Zeiss, Oberkochen, Germany), in which scaffold samples were freeze-dried for 24 h, followed by the coating of a thin layer of gold. The element distribution of Ca, P and N in SEM micrographs of scaffolds were examined using EDX elemental mapping. Compression testing was conducted on thicker scaffolds (40 layer, 14mm thick) with a strain rate of 2 mm/min, under wet condition at 37 ^{o}C and 5 samples were tested for each type of scaffolds.

***In vitro* photothermal performance of scaffolds**

The photothermal performance of wet scaffolds was investigated by irradiating scaffolds at power densities of 0.5 to 2.0 W·cm^{-2}. NIR laser was generated by an 808 nm high power multimode pump laser. The temperature and the corresponding thermal images of the irradiated sites were recorded on an infrared thermal imaging instrument (FLUKE Ti450, USA). The photothermal-conversion efficiency of BDPTP scaffolds were also investigated for 4 weeks by

monitoring the temperature increase of scaffolds after 10 min NIR irradiation.

In vitro release behavior of DOX and P24 peptide

To investigate *in vitro* release of DOX, pre-weighed scaffold samples were put in test tubes filled with PBS solutions supplemented with 0.02% sodium azide and the test tubes were put in a shaking water bath at 37 ^{o}C. At pre-determined time intervals, all of the test liquid was taken out and the concentration of DOX was measured using a fluorescence microplate reader at 480 nm. Afterwards, the same volume of fresh test liquid was added into the tube for continuous incubation. The release behaviour of DOX from scaffolds with and without NIR laser irradiation (10 min per day) was monitored up to 14 days, in which the NIR laser irradiation was applied every 24 h. For P24 peptide release test, similar experiments were conducted for up to 24 days and the test liquid was taken out everyday, followed by the addition of fresh test liquid. The concentration of released P24 peptide at each time point was measured using fluorescence microplate reader at 488 nm, in which P24 peptide conjugated with FITC was used as the target peptide. The NIR irradiation was also applied daily on BPTP and BDPTP scaffolds in first 4 days to investigate the effect of photothermal effect on P24 peptide release.

In vitro photothermal ablation of osteosarcoma cells

MG63 cell line was cultured in DMEM, (Gibco, USA) which was supplemented with 10% fetal bovine serum (Gibco, USA), 100 U/ml penicillin-streptomycin and 2 mM L-glutamine (Invitrogen, USA) and maintained in a humidified incubator at 37 ^{o}C with 5% CO_2. The medium was changed every 2 days. After cell confluence, MG63 cells were trypsinized and seeded on BDPTP scaffolds and other controls by dripping 50 µL of cell solution with a cell density of 1×10^{6}/mL on 10 mg of scaffold with a dimension of 5 mm × 5 mm × 1 mm, which contained 550

ng of DOX, followed by the addition of 500 μL of culture medium after 4 h incubation. The medium was changed every 2 to 3 days. The viability of MG63 cells after culturing 1, 4 and 7 days was investigated using live and dead kit assay (L3224, Thermofisher Inc.) and CCK8 assay was conducted to investigate the cell proliferation on multi-functional scaffolds. To evaluate the *in vitro* photothermal therapy efficiency, 50 μL of MG63 cells with a cell density of 1×10^6/mL were seeded on scaffolds and cultured for 1 or 3 days and further treated with/without NIR laser irradiation (1.2 $W\cdot cm^{-2}$, 5min) and then the live and dead assay were carried out.

In vivo tumor therapy

48 female balb/c nude mice (~15 g) were acquired and raised at 4-week old in the animal center of the Third affiliated hospital, South Medical University, China. MG63 cells (1×10^7 cell/site) suspended in PBS were injected subcutaneously into the neck of mice to develop the osteosarcoma model. When the tumors volume reached about 200 mm^3, the *in vivo* PTT was performed. The mice were divided into six groups (n = 5) randomly: (1) PTP group; (2) BPTP group; (3) BPTP + NIR group; (4) DPTP group; (5) BDPTP group; and (6) BDPTP + NIR group. A skin incision was made at the edge of the tumor, and the scaffolds with a dimension of 5 mm × 5 mm × 1.5 mm were then implanted into the center of the tumors. The volume of the tumors was monitored by a digital caliper every day during half a month after the corresponding treatments. The tumor volume was calculated according to the following formula: tumor volume (V) = (tumor length) × $(\text{tumor width})^2$ /2 – scaffold volume. The relative tumor volumes (Vr) were calculated as follows: $Vr = V/V_0$ (V_0 represents tumor volume on day 0). Thermal images of the irradiated mice were visualized on an infrared thermal imaging instrument (FLUKE Ti450, USA).

In vitro growth and osteogenic differentiation of rBMSCs

rBMSCs were cultured with Dulbecco's modified Eagle's medium/F-12, (DMEM/F-12, Gibco, USA) which was supplemented with 10% fetal bovine serum (Gibco, USA) and 100 U/ml penicillin-streptomycin and maintained in a humidified incubator at 37 ^{o}C with 5% CO_2. The medium was changed every 2 days. Afterwards, 100 uL of rBMSCs with a density of 1×10^5 were seeded on wet scaffolds which were treated with 10 min of NIR irradiation and immersed in PBS for 24 h beforehand, followed by the addition of 400 μL of medium after 4 h of culture. After 1 day of culture, rBMSC-scaffold constructs were fixed with 4% paraformaldehyde (PFA) and incubated with anti-vinculin for 1 h as well as corresponding secondary antibody (Alexa 488) for 30 min, and further incubated with DAPI (100 μL) and phalloidin 488 solution (100 μL) for 30 min. The stained F-actin filaments and vinculin adhesive plaques were then visualized using CLSM. By employing the same cell seeding procedure, the viability and proliferation of rBMSCs on scaffolds were also monitored on day 3 and in a 14-day culture period using CCK8 assay, respectively. The morphology of rBMSCs on scaffolds after 7-day culture was examined using SEM. To investigate the osteogenic differentiation, alkaline phosphatase (ALP) activity of rBMSCs on scaffolds was investigated, following the protocol used in our previous investigation. The extracts of scaffolds were also supplemented into the osteogenic media to culture cells for 21 days and the cell mineralization was visualized via Alizarin Red S (ARS) staining. After taking micrographs, 10% cetylpyridinium chloride was used to dissolve the nodules, and the absorbance was examined at 562 nm.

Osteogenic gene expression of rBMSCs

rBMSCs were seeded on scaffolds for 7 to 21 days and Trizol (Thermofisher Scientific, USA) was used to extract mRNA from the cells. The reverse transcription procedure was carried out by TaqMan MicroRNA Reverse Transcription Kit (Thermofisher Scientific, USA). qPCR Sybn

Green Master Mix (Thermofisher Scientific, USA), forward and reverse primers and cDNA were loaded onto a 96-well plate, and the RT-PCR procedure was performed in ABI 7900HT Sequence Detection System. The primer sequence is shown in Table S1. The qPCR data was analyzed using $2^{-\Delta\Delta Ct}$ method.

Construction of cranial defect models

All the animal surgical procedures were approved by the Animal Research Committee of South Medical University. Thirty-six male Sprague-Dawley rats (10 weeks old, body weight: 300-350 g) were used for experiments. The rats were anesthetized by intraperitoneal injection of pentobarbital, then a sagittal incision of 1.5-2.0 cm was made on the scalp. One full-thickness 5 mm-diameter defect was made on each side of craniums using an electric trephine drill. Then TP, PTP, BPTP, DPTP or BDPTP scaffolds (n = 5 for each group) which were irradiated by NIR laser for 10 min (to mimic the anti-cancer stage), were cut into implants with a diameter of 5 mm and a thickness of 1 mm, and implanted into cranial defects afterwards[40,41]. The soft tissues were re-positioned and sutured with 4-0 silk sutures to achieve primary closure. Sham surgery was also conducted. Each rat received an intraperitoneal injection of antibiotics post-surgery. Micro-CT evaluation and corresponding histomorphometric analyses were conducted after 2 and 3 months, respectively. After 3 months post-surgery, 30 rats were sacrificed, and obtained calvarias were scanned using micro-CT (Skyscan1176, Kontich, Belgium). The scanning was performed at a resolution of 18 μm and the images were acquired to reconstruct tomograms with 3D Creator software. The ratio of bone volume/tissue volume (BV/TV) and bone mineral density (BMD) were measured using CTAn image analysis software based on the micro-CT images.

Histological analysis

Cranias were retrieved, fixed, decalcified, dehydrated and defatted before embedding in paraffin, as previously described. Then, the samples were cut into 4-mm thick sections by a paraffin microtome (RM2125 RTS, Leica, Wetzlar, Germany). The sections were stained with the haematoxylin and eosin (H&E) and Masson's trichrome staining methods in accordance with the standard protocols[42]. For all types of stained sections, bone histomorphometric analysis was performed under a semi-automated digitizing image analyser system with a ZEISS Scope.A1(ZEISS, Germany).

Statistical analysis

Quantitative data are expressed as mean ± s.d. One-way ANOVA tests via Student's t tests were conducted and the data were indicated with (*) for probability less than 0.05 ($p < 0.05$).

Acknowledgments

This work was supported by Dongguan University of Technology High-level Talents (Innovation Team) Research Project (KCYCXPT201603), Youth Innovative Talent Project from the Department of Education of Guangdong Province, China (2016KQNCX168), Natural Science Foundation of Guangdong Province, China (2018A0303130019).

Conflicts of interest

There are no conflicts to declare.

Author contributions

C. Wang. and L. Mei. conceived the project. C. Wang., X. Xie., Z. He. and Q. Tong. conducted the scaffold fabrication, characterization, *in vitro* release/degradation test and *in vitro* cell culture. X. Ye., Y. Zhou conducted the *in vivo* anti-cancer study. Y. Zhao., H. Zhu., D. Cai. and D. Xie

conducted the *in vivo* experiments in rat cranial defects and analyzed the related data. C. Wang., B. Lu., M. Wang., Y. Wei., D. Xie. and L. Mei. contributed to the writing of the manuscript.

References

[1] Heck, R. K., Peabody, T. D., Simon, M. A. Strategy of primary malignancies of bone. CA-Cancer J Clin 56, 366-375 (2006).

[2] Ma, H. S., Luo, J., Sun, Z., Xia, L.G., Shi, M.C., Y,M. 3D printing of biomaterials with mussel-inspired nanostructures for tumor therapy and tissue regeneration. Biomaterials 111, 138 (2016).

[3] Pugazhendhi, A., Edison, TN. J. I., Velmurugan, BK., Jacob, J.A., Karuppusamy, I. Toxicity of doxorubicin (Dox) to different experimental organ systems.Life Sciences 200, 26-30 (2018).

[4] Jalili, N., Jaiswal M.K., Peak,CW., Cross, LM., Gaharwar,AK. Injectable nanongineered stimuli-responsive hydrogels for on-demand and localized therapeutic delivery. Nanoscle 9, 15379-15389 (2017).

[5] Zhou, Z.F., Sun, T.W., Chen, F., Zuo, D.Q., Wang, H.S., Hua, Y.Q., Cai, Z.D., Tan, J. Calcium hosate- hophoylated adenosine hybrid microspheres for anti-osteosarcoma drug delivery and osteogenic differentiation. Biomaterials 121, 1-14 (2017).

[6] Ma ,H., Jiang C., Hai, D., Luo,Y., hen,Y., Lv,F., Li, Z.F., Deng, Y. A bifunctional biomaterial with photothermal effect for tumor therapy and bone regeneration. Adv Funct Mater 26, 1197-1208 (2016).

[7] Tao, W., Zhu, X. B., Yu, X. H. Black phosphorus nanosheets as a robust delivery platform

for cancer theranostics. Adv Mater 29, 1603276 (2017).

[8] Yang, B., Yin, J., Chen, Y. , Shi, J. 2D black phosphorus reinforced 3D printed scaffolds: a stepwise countermeasure for osteosarcoma. Adv Mater 30, 1705611 (2018).

[9] Liu, C., Yao, W., Tian, M., Wei, J., Song, Q., Qiao, W. Mussel-inspired degradable antibacterial polydopamine/silica nanoparticle for rapid hemostasis, Biomaterials, 179: 83-95 (2018).

[10] Su A Park, Sang Jin Lee, Ji Min Seok, Jun Hee Lee, Wan Doo Kim, ll Keun Kwon. Fabrication of 3D Printed PCL/PEG Polyblend Scaffold Using Rapid Prototyping System for Bone Tissue Engineering Application. Journal of Bionic Engineering 15(3), 435-442(2018).

[11] Demirtaş, T. T., Irmak, G., Gümüşderelioğlu, M. A bioprintable form of chitosan hydrogel for bone tissue engineering. Biofabrication 9(3), 035003(2017).

[12] Luo, Y., Luo, G., Gelinsky, M., Huang, P., Ruan, C. 3D bioprinting scaffold using alginate/polyvinyl alcohol bioinks. Materials Letters 189, 295-298(2017).

[13] Heo, E. Y., Ko, N. R., Bae, M. S., Lee, S. J., Choi, B. J., Kim, J. H., Kim, H. K., Park, S. A. Kwon, K. Novel 3D printed alginate–BFP1 hybrid scaffolds for enhanced bone regeneration. Journal of Industrial and Engineering Chemistry 45, 61-67(2017).

[14] Wang, C., Zhao, Q.L., Wang, M. Cryogenic 3D printing for producing hierarchical porous and rhBMP-2-loaded Ca-P/PLLA nanocomposite scaffolds for bone tissue engineering. Biofabrication 9 025031 (2017).

[15] Ritter, J., Bielack, S. S. Osteosarcoma. Ann Oncol 21, 320-325 (2010).

[16] Tredan, O., Galmarini,C. M., Patel, K., Tannock, I. F. Drug resistance and the solid tumor microenvironment. J Natl Cancer I 99, 1441-1454 (2007).

[17]Yang, F., Wen, X., Ke, Q.F., Xie, X.T., Guo, Y. P. pH-responsive mesoporous ZSM-5 zeolites/chitosan core-shell nanodisks loaded with doxorubicin against osteosarcoma. Mater Sci & Eng C-Mater 85, 142-153 (2018).

[18] Robl, B., Botter, S. M., Pellegrini, G., Neklyudova, O., Fuchs, B. Evaluation of intraarterial and intravenous cisplatin chemotherapy in the treatment of metastatic osteosarcoma using an orthotopic xenograft mouse model. J Exp Clin Canc Res 35: 113(2016).

[19] Du, J. H., Xie, P., Lin, S. X., Wu, Y. Q., Zeng, D. L., Li, Y. L., Jiang, X. Q. Time-phase sequential utilization of adipose-derived mesenchymal stem cells on mesoporous bioactive glass for restoration of critical size bone fefects.ACS Appl Mater Inter 10, 28340-28350 (2018).

[20] Wang, L., Zhu, L. X., Wang, Z., Lou, A. J., Yang, Y. X., Guo, Y., Liu, S., Zhang, C. Development of a centrally vascularized tissue engineering bone graft with the unique core-shell composite structure for large femoral bone defect treatment. Biomaterials 175, 44-60 (2018).

[21] Liu, X. J., Yu, B., Huang, Q. L., Liu, R., Feng, Q. L., Cai, Q., Mi, S. L., In vitro BMP-2 peptide release from thiolated chitosan based hydrogel. Int J Biol Macromol 93: 314-321 (2016).

[22] Li, J., Jin, L., Wang, M., Zhu, S. & Xu, S., Repair of rat cranial bone defect by using bone morphogenetic protein-2-related peptide combined with microspheres composed of polylactic acid/polyglycolic acid copolymer and chitosan. BIOMED MATER 10 45004

(2015).

[23] Maayah, Z. H, Zhang, T., Forrest, .M. L., Alrushaid, S., Doschak, M. R., Davies, N. M., El-Kadi, A. O. S. DOX-Vit D, a novel doxorubicin delivery approach, inhibits human Oosteosarcoma cell proliferation by inducing apoptosis while inhibiting Akt and mTOR signaling pathways. Pharmaceutics 10, 144 (2018).

[24] Ma ,H., He, C., Cheng, Y., Yang, Z., Zang, J., Liu, J., Chen, X. Localized co-delivery of doxorubicin, cisplatin, and methotrexate by yhermosensitive hydrogels for enhanced osteosarcoma treatment. ACS Appl Mater Inter 7, 27040-27048 (2015).

[25] Al-Ahmady, Z. S., Al-Jamal, W. T., Bossche, J. V., Bui, T. T., Drake, A. F., Mason.A. J., Kostas. K. Lipid-peptide vesicle nanoscale hybrids for triggered frug release by mild hyperthermia in vitro and in vivo. ACS Nano 6, 9335-9346 (2012).

[26] Lopez-Noriega, A., Ruiz-Hernandez, E., Quinlan.E.,Storm, G., Hennink,W. E., O'Brien, F. J. Thermally triggered release of a pro-osteogenic peptide from a functionalized collagen-based scaffold using thermosensitive liposomes. J Control Release 187, 158-166 (2014).

[27] Yao, Q .Q., Liu,Y. X., S.B.,K.RT.,S.HL. Mesoporous silicate nanoparticles/3D nanofibrous scaffold-mediated dual-drug delivery for bone tissue engineering. J Control Release 279, 69-78 (2018).

[28] Ye, K., Liu, D., Kuang, H., Cai, J., Chen, W., Sun, B., Xia, L., Fang, B.Three-dimensional electrospun nanofibrous scaffolds displaying bone morphogenetic protein-2-derived peptides for the promotion of osteogenic differentiation of stem cells and bone regeneration. J Colloid Interf Sci 534, 625-636 (2019).

[29] Jaidev, L.R., Chatterjee, K. Surface functionalization of 3D printed polymer scaffolds to augment stem cell response. Materials Design 161, 44-54 (2019).

[30] Zhao, Y., Wang, H., Huang, H., Xiao, Q., Xu, Y., Guo, Z., Xie, H., Shao, J., Sun, Z., Han. W., Yu, X.F., Li, P., Chu, P.K. Surface Coordination of Black Phosphorus for Robust Air and Water Stability. Angew Chem Int Ed Engl 55, 5003-5007 (2016).

[31] Pei, D. D., Sun, J.L., Zhu, C.H., Tian, F.C., Jiao, K., Anderson, M.R., Yiu, C., Huang, C., Jin, C.X., Bergeron, B.E., Chen, J.H., Tay, F.R., Niu, L.N. Contribution of Mitophagy to Cell-Mediated Mineralization: Revisiting a 50-Year-Old Conundrum. Adv Sci (Weinh) 5, 1800873 (2018).

[32] Ma, C., Tian, X., Kim, J.P., Xie, D., Ao, X., Shan, D., Lin, Q., Hudock, M.R., Bai, X., Yang, J. Citrate-based materials fuel human stem cells by metabonegenic regulation. Proc Natl Acad Sci U S A 115, E11741-E11750 (2018).

[33] Qiu, M., Wang, D., Liang, W., Liu, L., Zhang, Y., Chen, X., Sang, D.K., Xing, C., Li, Z., Dong, B., Xing, F., Fan, D., Bao, S., Zhang, H., Cao, Y. Novel concept of the smart NIR-light-controlled drug release of black phosphorus nanostructure for cancer therapy. Proc Natl Acad Sci U S A 115, 501-506 (2018).

[34] Schneider, O. D., Weber, F., Brunner, T.J., Loher, S., Ehrbar, M., Schmidlin, P.R., Stark, W.J. In vivo and in vitro evaluation of flexible, cottonwool-like nanocomposites as bone substitute material for complex defects. Acta Biomater 5, 1775-1784 (2009).

[35] Rentsch, C., Rentsch, B., Heinemann, S., Bernhardt, R., Bischoff, B., Forster, Y., Scharnweber, D., Rammelt, S. ECM inspired coating of embroidered 3D scaffolds enhances calvaria bone regeneration. Biomed Res Int 2014 217078 (2014).

[36] Feng, P., Wu, P., Gao, C., Yang, Y., Guo, W., Yang, W., Shuai, C. A Multimaterial Scaffold With Tunable Properties: Toward Bone Tissue Repair. Adv Sci (Weinh) 5, 1700817 (2018).

[37] Bennett, S., Arumugam, M., Wilberforce, S., Enea, D., Rushton, N., Zhang, X.C., Best, S.M., Cameron, R.E., Brooks, R.A. The effect of particle size on the in vivo degradation of poly(d,l-lactide-co-glycolide)/alpha-tricalcium phosphate micro- and nanocomposites. Acta Biomater 45, 340-348 (2016).

[38] Amini, A. R., Wallace, J. S., Nukavarapu, S. P. Short-term and long-term effects of orthopedic biodegradable implants. J Long Term Eff Med Implants 21, 93-122 (2011).

[39] Zhou, W., Pan, T., Cui, H., Zhao, Z., Chu, P. K., Yu, X. F. Rediscovery of black phosphorus: bioactive nanomaterials with inherent and selective chemotherapeutic effects. Angew Chem Int Ed Engl. DOI: 10.1002/anie.201810878(2018)

[40] Qiu, Q. Q., Mendenhall, H. V., Garlick, D. S. & Connor, J., Evaluation of bone regeneration at critical-sized calvarial defect by DBM/AM composite. J Biomed Mater Res B Appl Biomater 81, 516-523 (2007).

[41] Wang, C. Z., Chen, S.M., Chen, C.H., Wang, C.K., Wang, G.J., Chang, J.K., Ho, M.L. The effect of the local delivery of alendronate on human adipose-derived stem cell-based bone regeneration. Biomaterials 31, 8674-8683 (2010).

[42] Wang, Y., Van Manh, N., Wang, H., Zhong, X., Zhang, X., Li, C. Synergistic intrafibrillar/extrafibrillar mineralization of collagen scaffolds based on a biomimetic strategy to promote the regeneration of bone defects. Int J Nanomedicine 11, 2053-2067 (2016).